Science of the Total Environment 697 (2019) 134093

Contents lists available at ScienceDirect

Science of the Total Environment

journal homepage: www.elsevier.com/locate/scitotenv

Factors controlling dissolved ^{137}Cs concentrations in east Japanese Rivers

Hideki Tsuji [a,*], Yumiko Ishii [a], Moono Shin [b], Keisuke Taniguchi [c], Hirotsugu Arai [c], Momo Kurihara [d], Tetsuo Yasutaka [e], Takayuki Kuramoto [f], Takahiro Nakanishi [g], Sangyoon Lee [h], Takuro Shinano [i], Yuichi Onda [j], Seiji Hayashi [a]

[a] National Institute for Environmental Studies, Fukushima Branch, 10-2 Fukasaku, Miharu, Tamura, Fukushima 963-7700, Japan
[b] Faculty of Food and Agricultural Sciences, Fukushima University, 1 Kanayagawa, Fukushima City, Fukushima Prefecture 960-1296, Japan
[c] Fukushima Prefectural Centre for Environmental Creation, 10-2 Fukasaku, Miharu, Tamura, Fukushima 963-7700, Japan
[d] National Institutes for Quantum and Radiological Science and Technology, 4-9-1 Anagawa, Inage-ku, Chiba-shi, Chiba 263-8555, Japan
[e] National Institute of Advanced Science and Technology, Research Institute for Geo-resources and Environment, 1-1-1 Umezono, Tsukuba, Ibaraki 305-8560, Japan
[f] Tokai University, School of Humanities and Culture, 4-1-1 Kitakaname, Hiratsuka, Kanagawa 259-1207, Japan
[g] Japan Atomic Energy Agency, Sector of Fukushima Research and Development, 45-169 Sukakeba, Kaihana, Haramachi-ku, Minamisoma City, Fukushima 975-0036, Japan
[h] National Agriculture and Food Research Organization, Western Region Agricultural Research Center, Shikoku Research Station, 2575 Ikano-cho, Zentsuji-shi, Kagawa 765-0053, Japan
[i] Hokkaido University, Research Faculty of Agriculture, Kita 9 Jo, Nishi 9, Kita-ku, Sapporo, Hokkaido 060-8589, Japan
[j] University of Tsukuba, Center for Research in Isotopes and Environmental Dynamics, 1-1-1 Tennodai, Tsukuba, Ibaraki 305-8572, Japan

HIGHLIGHTS

- Dissolved ^{137}Cs concentration decreased by one order of magnitude between 2012 and 2017.
- Normalized dissolved ^{137}Cs concentration well correlated with the building area ratio.
- Topographic wetness index generally predicted dissolved ^{137}Cs concentration.
- High dissolved ^{137}Cs concentration in urban areas cannot be explained by water quality.

GRAPHICAL ABSTRACT

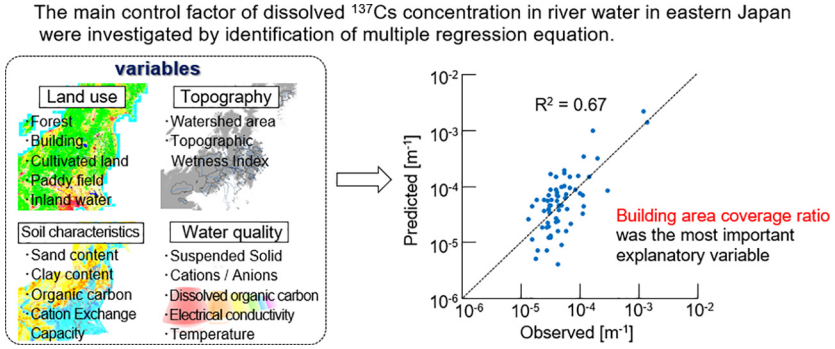

ARTICLE INFO

Article history:
Received 1 March 2019
Received in revised form 23 July 2019
Accepted 23 August 2019
Available online 26 August 2019

Editor: Christopher Bagwell

Keywords:
Fukushima Daiichi nuclear power plant

ABSTRACT

To investigate the main factors that control the dissolved radiocesium concentration in river water in the area affected by the Fukushima Daiichi nuclear power plant accident, the correlations between the dissolved ^{137}Cs concentrations at 66 sites normalized to the average ^{137}Cs inventories for the watersheds with the land use, soil components, topography, and water quality factors were assessed. We found that the topographic wetness index is significantly and positively correlated with the normalized dissolved ^{137}Cs concentration. Similar positive correlations have been found for European rivers because wetland areas with boggy organic soils that weakly retain ^{137}Cs are mainly found on plains. However, for small Japanese river watersheds, the building area ratio in the watershed strongly affected the dissolved ^{137}Cs concentration. One reason for this would be because the high concentrations of solutes, such as K^+ and dissolved organic carbon, discharged in urban areas would inhibit ^{137}Cs

* Corresponding author at: National Institute for Environmental Studies, Fukushima Branch, 10-2 Fukasaku, Miharu, Tamura, Fukushima 963-7700, Japan.
E-mail addresses: tsuji.hideki@nies.go.jp (H. Tsuji), ishii.yumiko@nies.go.jp (Y. Ishii), moono@agri.fukushima-u.ac.jp (M. Shin), taniguchi_keisuke_01@pref.fukushima.lg.jp (K. Taniguchi), arai_hirotsugu_01@pref.fukushima.lg.jp (H. Arai), kurihara.momo@qst.go.jp (M. Kurihara), t.yasutaka@aist.go.jp (T. Yasutaka), kuramoto.takayuki.f@tokai.ac.jp (T. Kuramoto), nakanishi.takahiro@jaea.go.jp (T. Nakanishi), is585@affrc.go.jp (S. Lee), shinano@chem.agr.hokudai.ac.jp (T. Shinano), onda@geoenv.tsukuba.ac.jp (Y. Onda), shayashi@nies.go.jp (S. Hayashi).

https://doi.org/10.1016/j.scitotenv.2019.134093

accident
River water
Topographic wetness index
Land use
Water quality
Multiple regression model

absorption to soil particles. A multiple regression equation was constructed to predict the normalized dissolved ^{137}Cs concentration with the topography, land use, soil component, and water quality data as explanatory variables. The best model had the building land use as the primary predictor. When comparing two multiple regression models in which the explanatory variables were limited to (1) the land use and soil composition and (2) the water quality, the water quality model underestimated the high normalized dissolve ^{137}Cs concentration in urban areas. This poor reproducibility indicates that the dissolved ^{137}Cs concentration value in urban areas cannot be solely explained by the solid-liquid distribution of ^{137}Cs owing to the influence of the water quality, but some specific ^{137}Cs sources in urban areas would control the dissolved ^{137}Cs concentration.

1. Introduction

Stock and flow of ^{137}Cs in aquatic environments have been investigated in many studies, mainly after the Chernobyl nuclear power plant (CNPP) and Fukushima Daiichi nuclear power plant (FDNPP) accidents. It is important to acquire data on ^{137}Cs dynamics in aquatic environments, integrate the data into our understanding of the behavior of ^{137}Cs in aquatic environments, and clarify the fundamental phenomena that drive ^{137}Cs migration and accumulation to allow the ^{137}Cs behavior in disaster areas to be predicted and to prepare for future nuclear disasters.

^{137}Cs in water mainly exists in dissolved and particulate phases. These two forms are conventionally distinguished by filtration, where the material that remains on the filter of 0.45–1.0 μm pore size is the particulate form and is the material contained in the filtrate is the dissolved form. Among the existing forms, dissolved ^{137}Cs is the most mobile and transferable, and understanding the dynamics of dissolved ^{137}Cs can allow ^{137}Cs contamination of crops and aquatic biota to be evaluated and predicted. After the CNPP accident, the dissolved ^{137}Cs concentration in environmental water was monitored at many sites, but quantification of the dissolved ^{137}Cs concentration was difficult because of the cumbersome procedures. Methods for measuring the dissolved ^{137}Cs concentration have been developed since the FDNPP accident, and investigation of the behavior of dissolved ^{137}Cs in river water (Ueda et al., 2013; Ochiai et al., 2015; Eyrolle-Boyer et al., 2016; Osawa et al., 2018), tributary and irrigation systems (Yoshikawa et al., 2014; Iwagami et al., 2017), pond water (Wakiyama et al., 2017; Konoplev et al., 2018), and seawater (Ramzaev et al., 2014; Fukuda et al., 2017) has increased. The results of these studies clarified some characteristic behaviors of dissolved ^{137}Cs in river water. The dissolved ^{137}Cs concentrations were found to be significantly and positively correlated with the ^{137}Cs inventories for watersheds 1–2 years after the FDNPP accident (Tsuji et al., 2015a, 2015b; Ochiai et al., 2015; Yoshimura et al., 2015). In addition, the dissolved ^{137}Cs concentrations were found to increase in summer (Tsuji et al., 2016; Wakiyama et al., 2017; Nakanishi and Sakuma, 2019) and be higher in river estuaries than inland along the same rivers (Kakehi et al., 2016; Onodera et al., 2017). The dissolved ^{137}Cs concentrations even increase or decrease after storms (Nagao et al., 2013; Tsuji et al., 2016).

Clarifying the factors that generally control the dissolved ^{137}Cs concentration in river water would require water samples to be collected from a wide area (to ensure that various terrains and geological characteristics are represented) and in the same time period (to exclude the effects of seasonal fluctuation and decay over time). Smith et al. (1998) assessed the effect of land cover on the dissolved ^{137}Cs concentrations in surface lake water in part of Great Britain for the same period and found that bogs, open shrub moors, and dense shrub moors had relatively strong explanatory powers for dissolved ^{137}Cs concentrations. Smith et al. (2004) assessed the factors that commonly affect the total ^{137}Cs concentrations in European rivers. They found that the coverage of the inland water area and the dominance of soils classed as sandy soil for a watershed were significantly and positively correlated with the total ^{137}Cs concentration, assuming that ^{137}Cs was mostly in the dissolved form. However, these ratios cannot be used to predict the dissolved ^{137}Cs concentrations in rivers around the FDNPP because the area around the FDNPP has higher annual precipitation, larger forest area, smaller farmland area (because of the steep topography), and higher degree of ^{137}Cs absorption to soil particles than the area around the CNPP, as mentioned in some reviews (Evrard et al., 2015; Konoplev et al., 2016). For example, urban areas are expected to strongly affect the dissolved ^{137}Cs concentrations around the FDNPP because the same amount of deposited ^{137}Cs causes higher dissolved ^{137}Cs concentrations in urban rivers than in forest rivers (Yamashita et al., 2015).

The studies of the dissolved ^{137}Cs behavior in river water after the FDNPP accident were conducted for limited areas and specific time periods, and the factors that affect the dissolved ^{137}Cs concentration in Japanese river water remain poorly understood. Therefore, in this study, we assessed the main factors that control the dissolved ^{137}Cs concentration in Japanese river water. We first measured the dissolved ^{137}Cs concentrations and water quality, such as the coexisting solute concentration, in rivers of eastern Japan centered at the FDNPP in August and September 2017. The factors that are correlated with the dissolved ^{137}Cs concentrations in the rivers were then investigated with the water quality data and data from a geographic information system (GIS) in which the relationship is expected. In addition, the main factors that control the dissolved ^{137}Cs concentration in river water were investigated by multiple regression analysis.

2. Materials and methods

2.1. Study site and watershed data

River water samples were collected from 66 points on 64 rivers 13–280 km from the FDNPP between 7 August and 13 September 2017 (Fig. 1). Some of the river watersheds were part of another river watershed (i.e., they have the same river system, Table 1). The effect of seawater mixing caused by the tide was negligible for each sample. The altitude is high in the northwest and low in the southeast of the study area. Spatially distributed mesh data and watershed area segmentation data were acquired using ArcGIS GIS software (version 10.5, ESRI, Redlands, CA, USA). The watersheds containing the sampling points were divided by tracing ridges using surface height grid data from the National Institute of Advanced Science and Technology using the global digital elevation model with spatial resolution of 10 m × 10 m. The 66 watersheds each covered between 3.2 and 3600 km^2 (Table 1).

The average ^{137}Cs inventory (^{137}Cs storage per unit area; Bq m^{-2}) for each watershed in July 2011 was calculated to be between 4.7 × 10^3 and 1.7 × 10^6 Bq m^{-2} mainly using the ^{137}Cs inventory distribution map reported by Kato et al. (2019). This dataset extends the ^{137}Cs inventory distribution of the third airborne survey by the Ministry of Education, Culture, Sports, Science and Technology, Japan (MEXT), based on the relationship between the measured value of the ^{137}Cs inventory and the air dose rate near the ground surface within 80 km radius from the FDNPP to the wider area for measurement of the fifth airborne survey by the MEXT conducted on June 2012. The ^{137}Cs inventory data for near sites 1–3 were missing from this dataset, but they were acquired from a ^{137}Cs inventory distribution map of the airborne

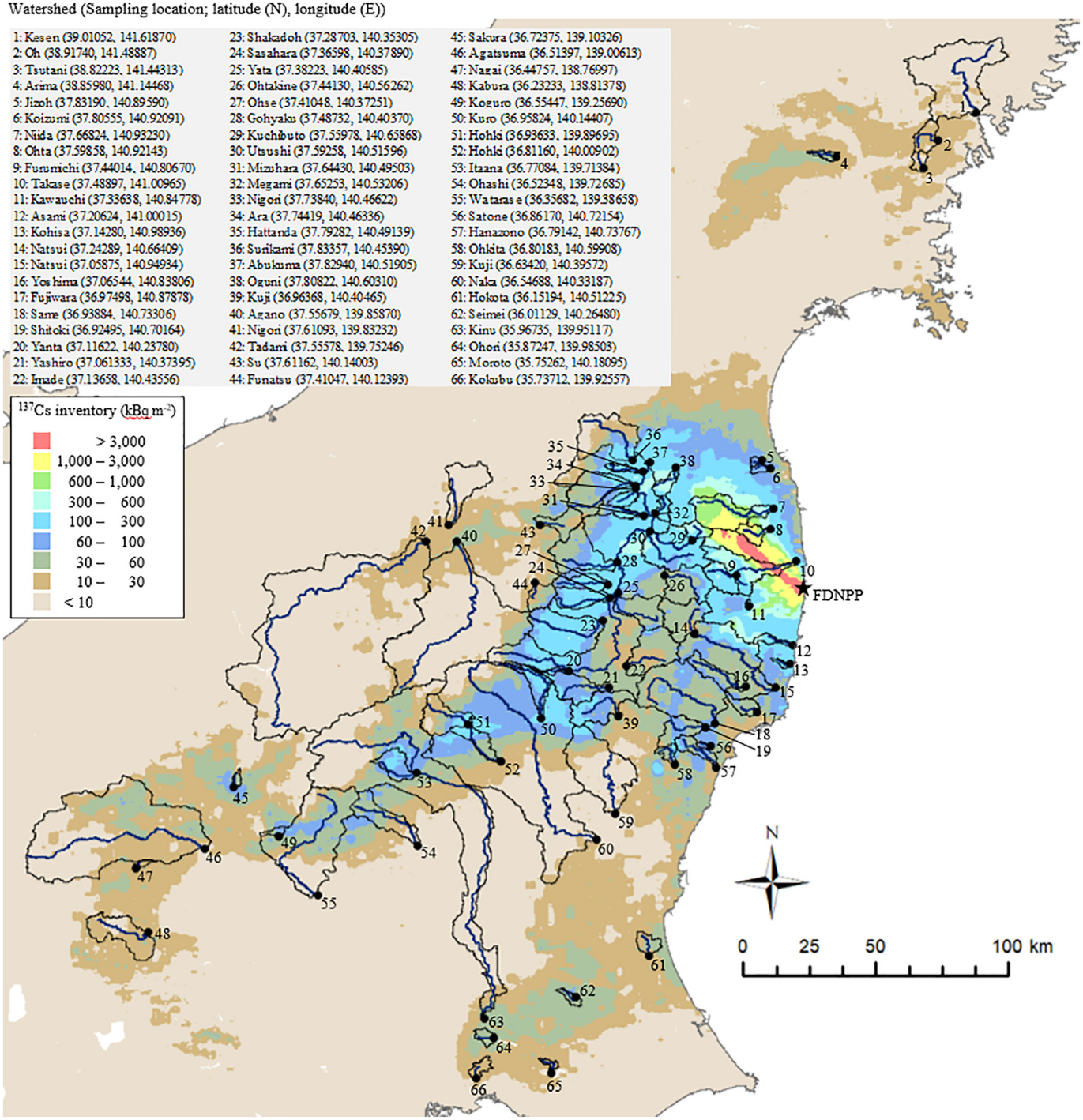

Fig. 1. Water sampling points (1–66) and watersheds. The watersheds were determined by the elevation map (National Institute of Advanced Science and Technology). The ^{137}Cs inventory on 2 July 2011 was a combination of Kato et al. (2019) and the fourth airborne survey of the MEXT (2011). The dataset values measured on October–November 2011 were decay-corrected to July 2011.

survey of each prefecture by the MEXT conducted in September 2011 and decay-corrected to July 2011.

2.2. Sampling and on-site processing

The 20–100 L river water sample was collected from a depth slightly higher than half of the river depth of several tens of centimeters to several meters using a Tempest DTW screw pump (Proactive Environmental Products, Bradenton, FL, USA) with a 2 mm screen or using a bucket lowered from a rope from the center of a bridge. Precipitation before the sampling days did not strongly affect the flow conditions, and the flow of each river was regarded as the baseflow condition. In the field, each water sample was passed through a 1 μm polypropylene cartridge filter (Tsuji et al., 2015a, 2015b) to remove particles and also through a second cartridge filter containing a nonwoven fabric impregnated with copper ferrocyanide with a pore size of 5 μm, which preferentially sorbs dissolved Cs (Yasutaka et al., 2016). The particle size distribution of the suspended solid (SS) in the river water sample was separately analyzed by laser diffraction (SALD3100, Shimadzu Co., Ltd., Tokyo, Japan). Particles smaller than 1 μm were detected at only five points with volume ratio of at most 2.2%. Hence, at these five points, the SS concentration might be slightly underestimated, but most of the <1 μm particles

Table 1
Analyte concentrations in the river water samples and other characteristics of the samples. The double sign of the dissolved ^{137}Cs concentrations are the counting errors of the detectors.

Site No.	River name	River system	Sampled date in 2017	Watershed topography[a]		Land use ratio (%)[b]					Averaged ^{137}Cs inventory (kBq m^{-2})[c]	Dissolved ^{137}Cs concentration (Bq m^{-3})	Normalized dissolved ^{137}Cs concentration ($\times 10^{-6}$ m^{-1})
				Area (km^2)	Topographic wetness index	Building	Forest	Paddy field	Cultivated land	Inland water			
1	Kesen	Kesen	09 Aug	510	7.3	2.3	91	2.3	2.1	0.4	4.7	0.79 ± 0.11	170
2	Oh	Oh	10 Aug	61	7.2	1.9	70	12	13	0.0	18	1.0 ± 0.2	58
3	Tsuya	Tsuya	10 Aug	28	8.1	0.9	87	6.7	5.1	0.0	11	0.4 ± 0.06	37
4	Arima	Kitakami	09 Aug	19	8.1	2.3	63	21	4.3	0.1	44	8.4 ± 0.8	190
5	Jizoh	Jizoh	07 Aug	11	7.9	2.4	73	7.6	4.1	0.4	74	11 ± 1	150
6	Koizumi	Koizumi	07 Aug	14	8.5	8.2	55	22	7.2	1.6	75	5.3 ± 0.5	71
7	Niida	Niida	23 Aug	190	7.7	0.9	77	10	9.5	0.3	890	32 ± 3	36
8	Ohta	Ohta	23 Aug	46	7.1	0.1	96	0.8	0.8	1.5	1700	120 ± 12	70
9	Furumichi	Ukedo	07 Aug	78	7.5	1.3	78	7.8	9.4	0.0	130	0.88 ± 0.18	6.6
10	Takase	Ukedo	23 Aug	260	7.4	1.4	83	6.6	6.5	0.4	730	29 ± 3	39
11	Kawauchi	Kido	07 Aug	3.2	7.2	0.0	93	0.8	0.2	0.0	140	1.0 ± 0.1	7.2
12	Asami	Asami	07 Aug	25	7.3	1.5	92	5.0	1.4	0.0	210	4.7 ± 0.5	23
13	Kohisa	Oh-hisa	07 Aug	10	7.6	1.9	75	8.3	3.7	0.4	120	11 ± 1	93
14	Natsui	Natsui	14 Aug	150	7.8	3.6	73	11	11	0.1	49	0.44 ± 0.10	8.9
15	Natsui	Natsui	07 Aug	650	7.6	4.4	81	7.2	4.7	0.5	74	2.0 ± 0.2	27
16	Yoshima	Natsui	07 Aug	86	7.4	1.0	92	5.2	0.5	0.0	57	1.1 ± 0.2	19
17	Fujiwara	Fujiwara	14 Aug	45	8.1	19	64	7.4	1.0	0.3	46	6.7 ± 0.7	150
18	Same	Same	22 Aug	440	7.3	1.1	87	5.9	5.0	0.2	49	2.2 ± 0.2	45
19	Shitoki	Shitoki	22 Aug	92	7.1	0.3	93	1.9	1.4	0.0	57	1.0 ± 0.2	18
20	Yanta	Abukuma	18 Aug	14	9.3	47	23	12	10	0.6	100	8.7 ± 0.9	84
21	Yashiro	Abukuma	23 Aug	130	8.3	8.3	61	18	7.2	1.0	83	3.7 ± 0.4	45
22	Imade	Abukuma	29 Aug	190	7.7	2.6	69	12	14	0.5	42	2.5 ± 0.2	58
23	Shakadoh	Abukuma	09 Aug	290	8.1	4.0	65	22	6.2	1.0	150	8.1 ± 0.8	54
24	Sasahara	Abukuma	07 Aug	97	9.0	14	44	35	2.6	1.8	130	5.7 ± 0.6	43
25	Yata	Abukuma	07 Aug	130	7.9	7.2	61	15	15	0.5	42	2.8 ± 0.3	66
26	Ohtakine	Abukuma	29 Aug	160	7.8	6.0	64	11	17	0.1	73	1.3 ± 0.2	18
27	Ohse	Abukuma	09 Aug	76	8.9	21	44	28	2.3	0.3	120	18 ± 2	150
28	Gohyaku	Abukuma	07 Aug	190	7.7	3.1	80	12	2.4	0.4	79	5.6 ± 0.6	70
29	Kuchibuto	Abukuma	09 Aug	39	7.7	1.1	70	7.5	20	0.0	420	4.4 ± 0.4	11
30	Utsushi	Abukuma	07 Aug	240	7.5	2.1	59	10	27	0.1	190	0.85 ± 0.09	4.5
31	Mizuhara	Abukuma	13 Sep	42	8.3	6.0	61	15	10	0.9	120	5.6 ± 0.6	45
32	Megami	Abukuma	13 Sep	30	7.7	7.1	51	16	24	0.1	190	3.0 ± 0.3	16
33	Nigori	Abukuma	10 Aug	35	8.5	16	57	13	8.0	0.3	140	11 ± 1	75
34	Ara	Abukuma	10 Aug	180	8.4	5.9	70	4.4	11	1.5	30	5.2 ± 0.5	170
35	Hattanda	Abukuma	10 Aug	23	9.4	17	42	11	23	0.7	190	13 ± 1	69
36	Surikami	Abukuma	10 Aug	240	7.0	0.4	95	0.3	2.0	1.7	40	1.7 ± 0.4	43
37	Abukuma	Abukuma	10 Aug	3600	8.2	8.0	59	16	12	1.4	110	4.3 ± 0.5	39
38	Oguni	Abukuma	08 Aug	40	7.6	3.8	65	8.8	20	0.1	350	7.3 ± 0.7	21
39	Kuji	Kuji	23 Aug	150	7.3	2.9	82	7.7	4.7	0.5	78	1.7 ± 0.2	22
40	Agano	Agano	07 Aug	12	7.4	2.2	84	7.8	3.3	2.0	9.2	0.72 ± 0.07	78
41	Nigori	Agano	07 Aug	160	7.7	2.7	80	11	3.2	2.0	5.4	0.80 ± 0.23	150
42	Tadami	Agano	07 Aug	2800	7.1	0.5	93	1.5	0.7	1.6	6.0	0.10 ± 0.05	16
43	Su	Agano	07 Aug	80	7.6	0.9	90	2.1	2.2	0.3	38	3.3 ± 0.3	86
44	Funatsu	Agano	11 Aug	63	7.4	1.9	85	10	2.6	0.6	37	0.19 ± 0.07	5.3
45	Sakura	Tone	10 Aug	12	7.1	0.0	98	0.0	0.0	0.0	47	2.7 ± 0.3	57
46	Agatsuma	Tone	10 Aug	1400	7.6	2.3	81	1.6	10	0.7	17	1.8 ± 0.2	100
47	Nagai	Tone	10 Aug	10	7.6	1.7	74	1.2	23	0.0	24	2.1 ± 0.2	88
48	Kabura	Tone	10 Aug	190	7.0	1.8	90	0.2	6.5	0.8	17	0.76 ± 0.21	45
49	Koguro	Tone	10 Aug	16	7.2	0.1	99	0.0	0.2	0.0	53	1.4 ± 0.2	26
50	Kuro	Naka	09 Aug	96	8.4	2.7	67	12	14	0.7	96	5.8 ± 0.6	61
51	Hohki	Naka	09 Aug	130	7.4	1.2	93	0.7	2.5	0.5	44	1.4 ± 0.3	33
52	Hohki	Naka	09 Aug	220	8.4	5.7	73	14	3.5	2.0	60	1.9 ± 0.3	32
53	Itaana	Tone	09 Aug	85	7.3	0.7	89	3.8	1.0	1.3	89	1.2 ± 0.2	13
54	Oh-ashi	Tone	09 Aug	150	7.3	2.2	86	6.2	2.8	1.1	37	0.88 ± 0.22	24
55	Watarase	Tone	09 Aug	650	7.1	5.6	87	0.6	1.6	1.2	33	1.5 ± 0.2	45
56	Satone	Satone	10 Aug	7.3	7.0	0.0	97	0.3	0.0	0.0	75	0.88 ± 0.29	12
57	Hanazono	Hanazono	10 Aug	59	7.4	2.0	89	5.7	0.9	0.6	63	5.4 ± 0.1	86
58	Ohkita	Ohkita	10 Aug	28	7.3	0.2	97	1.3	0.6	0.0	53	0.61 ± 0.14	12
59	Kuji	Kuji	10 Aug	390	7.1	2.3	83	5.6	6.6	0.9	20	1.1 ± 0.1	55
60	Naka	Naka	10 Aug	2200	8.5	6.3	63	18	7.8	2.0	43	1.6 ± 0.2	38
61	Hokota	Tone	10 Aug	45	10.5	6.3	18	11	62	0.0	29	9.8 ± 1.0	340
62	Seimei	Tone	08 Aug	21	10.2	27	21	18	23	1.8	51	16.0 ± 1.6	320
63	Kinu	Tone	07 Aug	1800	9.4	10	62	16	4.6	4.5	22	2.2 ± 0.4	96
64	Ohori	Tone	08 Aug	27	11.5	73	6.3	0.0	7.6	0.3	46	100 ± 10	2200
65	Moroto	Tone	08 Aug	15	10.1	15	24	17	24	0.9	15	15 ± 1	970
66	Kokubu	Tone	07 Aug	10.9	10.9	4.8	1.6	13	0.8	0.8	19	25 ± 3	1400

[a] Calculated from the elevation map by National Institute of Advanced Science and Technology.
[b] Calculated from land use map by Ministry of Land, Infrastructure and Transport and Tourism, Japan.
[c] Kato et al. (2019) and Ministry of Education, Culture, Sports, Science and Technology, Japan.

would not be trapped in the second cartridge filter because of its larger pore size. Therefore, we regarded the ^{137}Cs contained in the second cartridge filter as the dissolved fraction in the river water. The pH, electrical conductivity (not corrected for temperature), and water temperature were measured in the field using handheld meters (D-70, (Horiba, Kyoto, Japan) and Pro1030 (YSI, Yellow Springs, OH, USA)). A separate river water sample was passed through a membrane filter and the filtrate was used for measurement of the main cations (Ca^{2+}, K^{+}, Mg^{2+}, Na^{+}, and NH_4^{+}) and anions (Cl^{-}, NO_2^{-}, NO_3^{-}, PO_4^{3-}, and SO_4^{2-}) in the laboratory using an ICS-1600 high-performance liquid chromatograph (Thermo Fisher Scientific, Waltham, MA, USA). The dissolved organic carbon (DOC) concentration was measured using a TOC-L total organic carbon analyzer (Shimadzu, Kyoto, Japan). Another separate water sample was passed through a Whatman GF/F filter (GE Healthcare Life Sciences, Chicago, IL, USA) with 0.7 μm pores in the laboratory to determine the SS concentration. The GF/F filter with the SS attached was dried at 105 °C in an oven for >4 h, and the mass of SS attached to the filter was then calculated by subtracting the dry weight of the used filter from the dry weight of the unused filter.

2.3. Analysis of the ^{137}Cs radioactivity

The ^{137}Cs radioactivity in the cartridge filters used to trap dissolved radiocesium were determined using GC2520-7500SL, GC4020-7500SL, and GC4020 coaxial high-purity germanium detectors (Canberra Japan, Tokyo, Japan) and Spectrum Explorer software (Canberra Japan). The instruments were calibrated using MX033U8PP (The Japan Radioisotope Association, Tokyo, Japan) as a standard volume radioactivity source. The ^{137}Cs radioactivity of each sample was decay-corrected to the sampling day. The relative uncertainty for the measurements using the instruments was 3.8%, and this was confirmed by proficiency tests conducted by the Japanese National Institute of Advanced Science and Technology. The detection limit was defined as three times the standard deviation (i.e., 3σ) of the measured ^{137}Cs radioactivity. The ^{134}Cs concentrations were also measured, but they were below the detection limit for 63 of the 66 cartridge filters.

2.4. GIS dataset and analysis

The factors that are highly correlated with $^{137}Cs_{\_dis\_norm}$ were extracted by single correlation analysis. As factors that are expected to be correlated with the dissolved ^{137}Cs ($^{137}Cs_{_dis}$) concentration, the topography, land use, and soil characteristics were chosen as candidate factors. As topographic data, the wetness of the watershed can affect the $^{137}Cs_{\_dis}$ concentration because extension of the flooding area would promote dissolution of ^{137}Cs from ^{137}Cs-containing particles on the surface. Accordingly, the average wetness of each watershed of the observation point was assessed using the topographic wetness index (TWI) calculated using the elevation data from the global digital elevation model using the equation (Moore et al., 1991).

$$\mathrm{TWI} = \ln\left(FA/\tan(slope)\right) \quad (1)$$

where FA is the watershed area (km^2) and $slope$ is the slope determined from the difference between the elevation values for the relevant mesh data. A higher TWI indicates a wetter condition of the surface by a shallow groundwater level and also that the terrain is flatter. The distribution of the TWI values was calculated with the same resolution as the elevation data, and the average value for each watershed was calculated to be between 7.0 and 11.8 (Table 1).

The land use was considered as a candidate factor because the main ^{137}Cs source would be different depending on the land use, and drainage from urban and farming activities also has a significant effect on the river water quality. As an index of the land use, we calculated the land use area ratios of the percentage of the total area coverage of major land use (forest, buildings, cultivated land, paddy fields, and inland water) in the watershed to the complete watershed area (Table 1) using the land use segmentation mesh data with a resolution of 100 m × 100 m from the Japanese Ministry of Land, Infrastructure, Transport, and Tourism.

Some characteristics of the soil data were also considered, because the soil particle size and soil organic carbon content can affect the adsorption capacity of ^{137}Cs to soil particles. The cation exchange capacity (CEC) of soil can also influence the $^{137}Cs_{\_dis}$ concentration because it indicates the absorptivity of ^{137}Cs ions to soil particles. Accordingly, the watershed-averaged carbon contents, sand contents, clay contents, and CEC for the top 5 cm soil layer were calculated using Soilgrids data (World Soil Information database) with a resolution of 250 m × 250 m.

When comparing the $^{137}Cs_{\_dis}$ concentrations at many points, it is common to normalize the $^{137}Cs_{\_dis}$ concentration by dividing these values by the ^{137}Cs inventory in the watershed to eliminate the difference of the magnitude of ^{137}Cs deposition in each watershed. This normalized value is known as the entrainment coefficient (Garcia-Sanchez and Konoplev, 2009; Konoplev et al., 2016). Delmas et al. (2019) showed that averaged ^{137}Cs inventory in the whole watershed is effective for predicting the dissolved ^{137}Cs concentration. In this study, the $^{137}Cs_{\_dis}$ concentration was normalized by dividing it by the averaged ^{137}Cs inventory in each watershed on June 2011 (Kato et al., 2019), and this concentration is defined as the normalized dissolved ^{137}Cs concentration ($^{137}Cs_{_dis_norm}$). This ^{137}Cs inventory dataset was used for normalization because no dataset was available for the ^{137}Cs inventory after 2011 and this dataset is based on the actual ^{137}Cs inventory and covers the range of this study area. Area-wide decontamination mainly performed after 2012 reduced the ^{137}Cs inventory faster than natural nuclear decay in the agricultural land and residential area near the FDNPP. However, we considered that decontamination would not significantly affect comparison of $^{137}Cs_{\_dis\_norm}$ among the locations because the proportion of agricultural and residential land in the decontaminated watershed was not higher than that of forests (Table 1). In addition, the ^{137}Cs inventory of the non-decontaminated location within an 80 km region from the FDNPP in 2016 was found to have decreased from that in 2011 at almost the same speed as natural nuclear decay regardless of the location (Mikami et al., in press).

2.5. Multiple regression equation

We analyzed the main controlling factors and their contribution to the $^{137}Cs_{\_dis}$ concentration by the generalized linear model (GLM). We constructed three types of equations.

For the first equation, all of the variables shown in Table 1 and Supplemental Table 1 (topography, land use, soil characteristics, and water quality data) were nominated as candidate explanatory variables. Some variables were excluded in advance if they were highly correlated with another variable ($r > 0.7$) or have a mechanism that is highly substitutable for other variables. Specifically, the excluded data from the candidate variables were the TWI (substituted by the building area ratio), forest area ratio (substituted by the building area ratio), and cation/anion concentrations (substituted by the electrical conductivity (EC)). We call this model the "all parameter model".

For the second equation, the candidates explanatory variable were limited to only the GIS data of the topography, land use, and soil characteristics. This equation mainly reflects the contribution of the ^{137}Cs source in the watershed to the $^{137}Cs_{\_dis}$ concentration. We call this model the "GIS model".

For the third equation, the candidate explanatory variables were limited to the water quality with the solute concentration data. This equation reflects the influence of the distribution process between the solid and liquid phases of ^{137}Cs affected by the water quality. We call this model the "water quality model".

Because the ranges of the variables were different, each variable was standardized to an average of 0 and variance of 1 as pre-processing to

compare each contribution by the coefficients. Multiple regression models were generated with all term combination subsets, and the best model was selected by the Akaike information criterion (AIC). The smaller the AIC score, the better the balance between the goodness of fit of the model and the small number of parameters. Therefore, the equation with the lowest AIC score was considered to be the "best" model.

To identify the multiple regression equation of $^{137}Cs_{\_dis\_norm}$, $^{137}Cs_{\_dis\_norm}$ was logarithmically converted to the objective variable considering that the distribution of the $^{137}Cs_{\_dis\_norm}$ values (Table 1) was significantly different from a normal distribution. Therefore, the multiple regression equation has the following structure:

$$\ln\left({}^{137}Cs_{\_dis\_norm}\right) = \Sigma_a^i \cdot x_i + b \quad (2)$$

where $^{137}Cs_{\_dis\_norm}$ is the normalized dissolved ^{137}Cs concentration [m^{-1}], x_i is an explanatory variable, a_i is the coefficient of variable x_i, and b is the intercept. The GLM analysis was performed with R (version 3.5.2, R Core Team, 2018) using the MuMIn package for model selection.

3. Results and discussion

3.1. Dissolved ^{137}Cs concentration and water quality

The $^{137}Cs_{\_dis}$ radioactivity concentrations (Bq m^{-3}; hereafter, merely describe as "$^{137}Cs_{\_dis}$ concentrations") in the river water samples were 0.40–120 Bq m^{-3} (Table 2) and the concentrations tended to be higher near the FDNPP than farther from the FDNPP. The $^{137}Cs_{\_dis}$ concentrations at the 66 sampling sites were plotted against the average ^{137}Cs inventories for the watersheds, and a significant positive correlation (R^2 = 0.48, slope 5.8 × 10^{-5} m^{-1} with 95% confidence interval of 4.6–7.0 × 10^{-5} m^{-1}) was found using the least squares method (Fig. 2). Each measured $^{137}Cs_{\_dis}$ concentration was therefore normalized and the $^{137}Cs_{\_dis\_norm}$ concentrations were calculated to be 4.5 × 10^{-6} to 2.2 × 10^{-3} m^{-1}. The data points deviating from the regression line at the upper left part of Fig. 2 (watersheds 64–66) had relatively high building area ratios. The data points deviating from the regression line at the lower left are watersheds 42 and 44, which were dominated by forest.

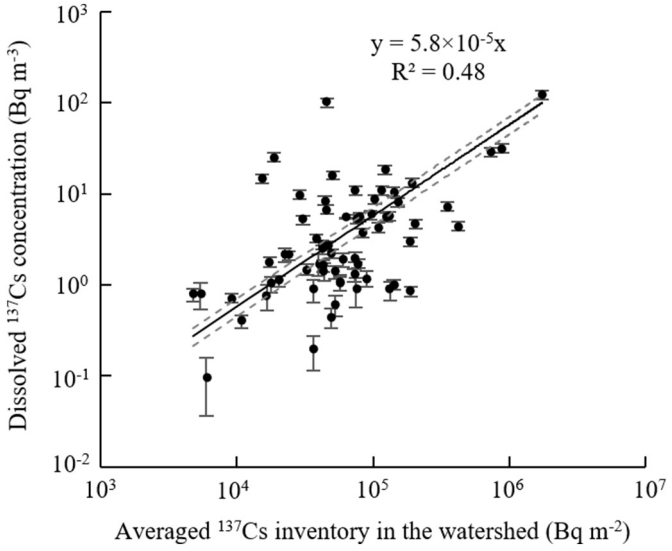

Fig. 2. Dissolved ^{137}Cs concentrations in river water plotted against the average ^{137}Cs inventories for the watersheds (log–log scale). The error bars indicate the detector counting errors. The dashed lines indicate the upper and lower 95% confidence intervals. Note that the graph is displayed in a logarithmic axis, but the approximate equation is a proportional equation and the correlation coefficient value (r) is based on linear regression analysis.

The latter data points had quite high levels of uncertainty because the ^{137}Cs concentrations were low, meaning that the counting errors (relative errors) were large. The $^{137}Cs_{\_dis\_norm}$ concentrations were less than those observed around the CNPP a few years after the accident (1.0 × 10^{-3} to 6.6 × 10^{-3} m^{-1}) (Konoplev et al., 2016). This difference indicates that the proportion of discharged ^{137}Cs as the dissolved form to the ^{137}Cs storage in the watershed was less in areas around the FDNPP compared with areas around the CNPP.

In previous studies, the lines describing the relationship between the $^{137}Cs_{\_dis}$ concentration and ^{137}Cs inventory had slopes of 4.8 × 10^{-4} m^{-1} (Tsuji et al., 2015a, 2015b), 2.7 × 10^{-4} m^{-1} in summer

Table 2
Correlation coefficients of the relationships between the normalized dissolved ^{137}Cs concentrations and characteristics of water from Japanese and European rivers. The meanings of the symbols are: * significant at the 5% level; ** significant at the 1% level.

Parameter		Japanese rivers (this study), n = 66		European rivers, n = 12[a]	
		Range in parameter	Correlation coefficient	Range in parameter	Correlation coefficient
Water quality	Water temperature, °C	17–35	0.42**		
	Electrical conductivity, mS m^{-1}	4.6–95	0.38**		
	pH	2.8–8.5	−0.05		
	Suspended solid concentration, g m^{-3}	2.1–37	0.22		
	NH_4^+ concentration, g m^{-3}	0–1.6	0.06		
	K^+ concentration, g m^{-3}	0.52–10	0.47**		
	Na^+ concentration, g m^{-3}	2.4–140	0.26*		
	Mg^{2+} concentration, g m^{-3}	0.56–14	0.30*		
	Ca^{2+} concentration, g m^{-3}	3.6–84	0.25*		
	Cl^- concentration, g m^{-3}	1.3–160	0.30*		
	NO_3^- concentration, g m^{-3}	0.51–31	0.22		
	SO_4^{2-} concentration, g m^{-3}	1.9–330	0.05		
	Dissolved organic carbon concentration, g m^{-3}	0.6–6.3	0.42**		
Land use[a]	% of forest areas in watershed	4.8–99	−0.63**	9.3–90	0.46
	% of building area in watershed	0–73	0.82**	no data	
	% of inland water in watershed	0–4.4	0.004	0–23	0.75**
	% of paddy field in watershed	0–37	−0.09	no data	
	% of cultivated land in watershed	0–62	0.17	0.2–89	−0.41
Soil	Mean % carbon content of soils	15–32	−0.32**	1.4–23	0.53*
	% of soils classed as sandy	36–45	−0.17	5.0–91	0.78**
	% of soils classed as clay	14–24	0.52**	0–14	0.08
	Cation exchange capacity of soil, meq kg^{-1}	25–51	−0.37**	no data	
Topography	Watershed area, km^2	3.2–3.6 × 10^3	−0.10	4.0 × 10^3–1.8 × 10^5	−0.22
	Topographic Wetness Index	7.0–12	0.74**	3.2–8.2	0.30

[a] Smith et al. (2004).

2012 (Ochiai et al., 2015), 1.3×10^{-4} m^{-1} in early winter 2012 (Yoshimura et al., 2015), and 2.1×10^{-4} m^{-1} in summer 2013 (Ochiai et al., 2015). The data used to give these slopes were all for measurements made within 100 km of the FDNPP. Plotting only the data for the 42 watersheds within 100 km of the FDNPP in this study gave a slope of 6.3×10^{-5} m^{-1}, which was almost the same as the slope for all 66 watersheds ($R^2 = 0.51$, slope 5.8×10^{-5} m^{-1} with 95% confidence interval of 4.9–6.7 $\times 10^{-5}$ m^{-1}). The relationship between the ^{137}Cs inventory and $^{137}Cs_{\_dis}$ concentration was therefore applicable further than 100 km from the FDNPP. The changes in the slope over time indicated that the dissolved ^{137}Cs concentrations in the river water decreased by one order of magnitude between 2012 and 2017. This decrease was faster than that predicted by the ^{137}Cs half-life (30.1 years). However, it has been reported that the annual runoff proportion of ^{137}Cs to the ^{137}Cs storage in the watershed after the FDNPP accident was at most 0.1% order of magnitude (Ueda et al., 2013; Tsuji et al., 2019), so ^{137}Cs storage did not remarkably change from the initial ^{137}Cs fallout. Accordingly, this decrease indicates that the proportion of ^{137}Cs that is easily washed away or ^{137}Cs that supplies dissolved ^{137}Cs to the land decreased over the 5 years.

The individual data of the water quality along with the solute concentrations are given in Supplemental Table 1. The NO_2^- and PO_4^{3-} concentrations were below the detection limits (0.01 g m^{-3} for both) at all of the sampling points. The NH_4^+ concentrations were below the detection limit (0.006 g m^{-3}) at 24 sampling points. The SS concentrations were 2.1–33 g m^{-3}. The pH values at most of the sampling sites were 5.7–8.5, which can be regarded as approximately neutral. However, the river Su water (site 43 in Fig. 1) was acidic (pH 2.8). The electrical conductivities were 5.1–95 mS m^{-1}, and they were higher in urban areas (e.g., sites 17 and 66) and at the coast (site 13) than elsewhere. The water temperatures were 17–35 °C, and they were higher in the southern lowland area than elsewhere.

3.2. Relationships between the normalized dissolved ^{137}Cs concentrations and environmental factors

3.2.1. Water quality

The water temperature was significantly and positively correlated with the $^{137}Cs_{\_dis\_norm}$ concentration (Table 2). An increase in the water temperature can increase the $^{137}Cs_{\_dis\_norm}$ concentration by shifting the equilibrium between ^{137}Cs in the solid and dissolved phases towards the dissolved phase (Tertre et al., 2005; Wu et al., 2009).

The K^+ and DOC concentrations were significantly and positively correlated with the $^{137}Cs_{\_dis\_norm}$ concentration at the 1% level, the Na^+, Mg^{2+}, Ca^{2+}, and Cl^- concentrations were significantly correlated with the $^{137}Cs_{\_dis\_norm}$ concentration at the 5% level, and the NH_4^+, NO_3^-, and SO_4^{2-} concentrations showed almost no correlation with the $^{137}Cs_{\_dis\_norm}$ concentration. Generally, K^+ and NH_4^+ promote elution of ^{137}Cs from river sediment because they readily exchange with ^{137}Cs at the frayed edge sites on soil particles (Wauters et al., 1996; Staunton and Roubaud, 1997). The poor correlation between the $^{137}Cs_{\_dis\_norm}$ concentration and NH_4^+ concentration was probably because the NH_4^+ concentrations were low compared with those of other ions, such as K^+. The $^{137}Cs_{\_dis\_norm}$ concentration was well correlated with the DOC concentration, probably because DOC can increase the $^{137}Cs_{\_dis}$ concentration by inhibiting sorption of dissolved ^{137}Cs to soil particles (Staunton et al., 2002). The concentrations of ions that can inhibit ^{137}Cs sorption can be represented by the electrical conductivity. It has been found that the $^{137}Cs_{\_dis}$ concentration increases as the electrical conductivity increases in agricultural water systems near the FDNPP (Tsukada et al., 2017; Eguchi, 2017).

There was almost no correlation between the $^{137}Cs_{\_dis\_norm}$ concentration and pH value because the water samples from most of the rivers were almost pH neutral. There was also no significant correlation between the SS concentration and $^{137}Cs_{\_dis\_norm}$ concentration. However, the SS concentration has been found to affect the behavior of dissolved ^{137}Cs in previous studies. Eyrolle-Boyer et al. (2016) found that the $^{137}Cs_{\_dis}$ concentration to ^{137}Cs concentration in the SS ratio increased as the SS concentration increased. Tsuji et al. (2016) found that the $^{137}Cs_{\_dis}$ concentration increased as the SS concentration increased in a forest river. Naulier et al. (2017) found that there was a change in the main SS components from organic matter to soil minerals and the $^{137}Cs_{\_dis}$ concentration was affected by this shift. Different $^{137}Cs_{\_dis}$ concentrations under storm runoff conditions and baseflow conditions have been found (Nagao et al., 2013; Tsuji et al., 2016), meaning that the SS concentration could affect the $^{137}Cs_{\_dis}$ concentration when a river becomes turbid after rain.

3.2.2. Land use

The building area ratio was significantly and positively correlated with the $^{137}Cs_{\_dis\_norm}$ concentration and had a higher correlation coefficient ($r = 0.82$, Fig. 3a) than the correlations with the other factors. The forest area ratio and $^{137}Cs_{\_dis\_norm}$ concentration were negatively correlated. Accordingly, the $^{137}Cs_{\_dis\_norm}$ concentrations were higher in urban areas than forest areas.

The correlation between the $^{137}Cs_{\_dis\_norm}$ concentration and the building area ratio would have been caused by the high water temperatures in urban areas and the concentrations of solutes in water discharged into rivers in urban areas (Table 3). This phenomenon where the temperature peculiarly increases in the urban area compared with the peripheral part is called the “urban heat island phenomenon”, which occurs because of human activities in the urban area. As another possible factor, road dust is an important contributor of SS in urban

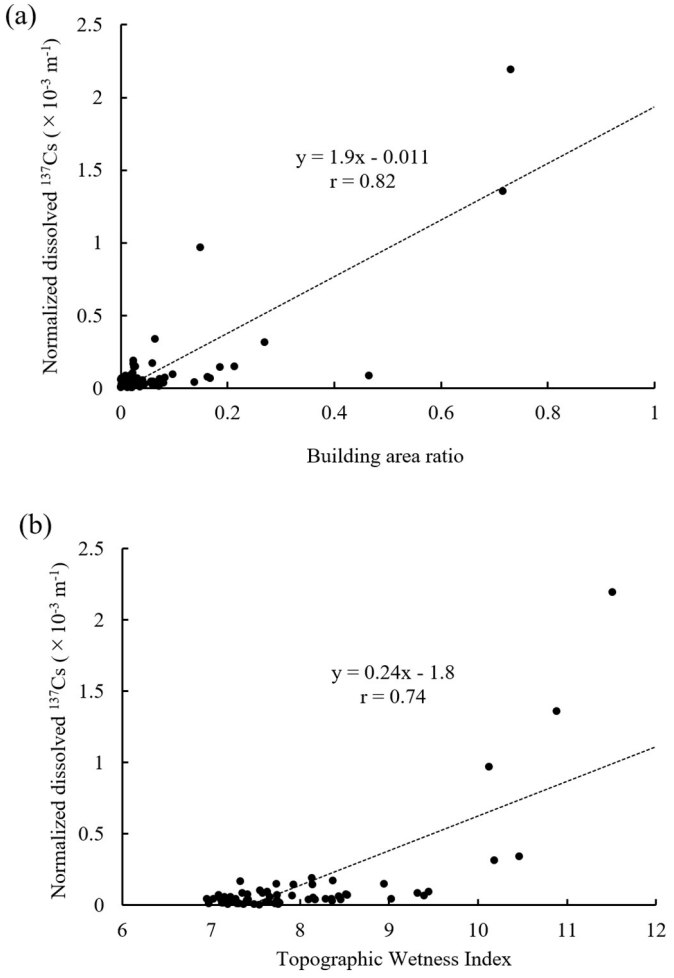

Fig. 3. Relationships between the normalized dissolved ^{137}Cs concentration and the (a) building area ratio and (b) topographic wetness index.

Table 3
Correlation matrix of the relationships between the factors. The abbreviations mean: WT, water temperature; EC, electrical conductivity; SS, suspended solid; DOC, dissolved organic carbon; CEC, cation exchange capacity; and TWI, topographic wetness index. The symbols mean: *, significant at the 5% level; **, significant at the 1% level; †, positively correlated with the normalized dissolved ^{137}Cs concentration at the 1% level; §, negatively correlated with the normalized dissolved ^{137}Cs concentration at the 1% level.

	WT†	EC†	pH	SS conc.	NH_4^+ conc.	K^+ conc.†	Cl^- conc.	DOC conc.†	Forest area ratio§	Building area ratio†	Inland water area ratio	Paddy field area ratio	Cultivated land area ratio	Carbon content§	Sandy soil ratio	Clay soil ratio†	CEC of soil§	Watershed area	TWI†
WT†	1																		
EC†	0.44**	1																	
pH	0.10	0.05	1																
SS conc.	0.20	0.22	−0.07	1															
NH_4^+ conc.	0.23	0.10	0.17	0.21	1														
K^+ conc.†	0.49**	0.69**	−0.08	0.45**	0.27	1													
Cl^- conc.	0.26*	0.84**	−0.09	0.19	0.11	0.65**	1												
DOC conc.†	0.27*	0.34**	0.13	0.27*	0.27	0.57**	0.21	1											
Forest area ratio§	−0.54**	−0.54**	0.00	−0.38**	−0.17	−0.77**	−0.42**	−0.46**	1										
Building area ratio†	0.47**	0.54**	0.03	0.16	0.12	0.56**	0.47**	0.35**	−0.78**	1									
Inland water ratio	0.41**	0.02	−0.06	−0.06	0.09	0.02	−0.01	−0.07	−0.11	0.07	1								
Paddy field area ratio	0.35**	0.11	0.02	0.14	0.07	0.35**	0.08	0.21	−0.52**	0.10	0.28*	1							
Cultivated land area ratio	0.18	0.24	−0.02	0.47**	0.10	0.60**	0.13	0.29*	−0.60**	0.14	−0.15	0.22	1						
Carbon content of soil§	−0.49**	−0.55**	−0.16	−0.10	−0.18	−0.49**	−0.36**	−0.49**	0.55**	−0.44**	−0.20	−0.34**	−0.17**	1					
Sandy soil ratio	−0.13	0.00	0.22	0.00	0.36*	−0.01	0.02	0.16	0.33**	−0.34**	−0.14	−0.32**	0.03	0.10	1				
Clay soil ratio†	0.54**	0.57**	0.01	0.16	−0.20	0.45**	0.37**	0.26*	−0.64**	0.66**	0.26*	0.27*	0.14	−0.69**	−0.56**	1			
CEC of soil§	−0.46**	−0.54**	0.06	−0.29*	−0.03	−0.59**	−0.43**	−0.21	0.77**	−0.54**	−0.05	−0.53**	−0.40**	0.59**	0.28*	−0.56**	1		
Watershed area	0.09	−0.09	−0.07	0.37	−0.09	−0.08	−0.08	−0.02	0.07	−0.08	0.49**	0.06	−0.08	0.03	−0.06	0.05	0.15	1	
TWI†	0.53**	0.51**	−0.06	0.33**	0.21	0.76**	0.41**	0.44**	−0.93**	0.80**	0.23	0.41**	0.48**	−0.54**	−0.34**	0.65**	−0.69**	−0.04	1

rivers (Carter et al., 2003), and it is also an important source of dissolved ^{137}Cs in river water because ^{137}Cs in road dust is generally relatively soluble. Yamashita et al. (2015) found that road dust was a major source of particulate ^{137}Cs in an urban river in watershed 64. However, Murakami et al. (2017) found that road dust made limited contributions to the $^{137}Cs_{\_dis\_norm}$ concentrations in the rivers in watersheds 27, 28, and 34. The building area ratios were smaller in the rivers of the latter report than in the river of the former report (Table 1), indicating that road dust is likely to be an important source of dissolved ^{137}Cs only when buildings occupy a large proportion of the watershed.

The negative correlation between the forest area ratio and $^{137}Cs_{\_dis\_norm}$ concentration can be explained in the opposite way to the positive correlation between the building area ratio and $^{137}Cs_{\_dis\_norm}$ concentration, which could also be explained by the relatively low electrical conductivity of the water in watersheds dominated by forest.

The agricultural area (paddy fields and cultivated land) ratio showed a poor correlation with the $^{137}Cs_{\_dis\_norm}$ concentration, because the agricultural area occupied much less area than forest. The cultivated land area ratio was significantly correlated with the K^+ and DOC concentrations, probably because of fertilizer discharge, but the effect of agricultural activities on the $^{137}Cs_{\_dis}$ concentration was small compared with the effect of urban areas. However, in some paddy fields near the FDNPP, the paddy fields have been found to behave as sinks for dissolved ^{137}Cs because ^{137}Cs sorbs to the decontaminated soil when irrigation water is applied (Shin et al., 2019).

The inland water area ratio was poorly correlated with the $^{137}Cs_{\_dis\_norm}$ concentration, which differs from European rivers (Smith et al., 2004). This difference is because some watersheds in Finland (where the inland water area ratios are relatively high, up to 23%) were used in the study of European rivers, but the water area ratio was relatively low in our study area (up to 4.5%) because of the relatively steep topography and the buildings mainly being in lowland areas.

3.2.3. Soil components

The carbon content and CEC of soil were negatively correlated with the $^{137}Cs_{\_dis\_norm}$ concentration. The correlation between the carbon content and the $^{137}Cs_{\_dis\_norm}$ concentration was unexpected because organic soil generally weakly retains ^{137}Cs (Hilton et al., 1993). A positive correlation between organic-rich boggy soil and the $^{137}Cs_{\_dis\_norm}$ concentration was found in Great Britain (Smith et al., 1998). This discrepancy can be mainly explained by the soil with high carbon contents in our study area mostly being in forested mountainous areas, meaning that the forest (a weak supplier of dissolved ^{137}Cs) characteristics were more important than the carbon content of the soil.

The clay soil ratio was positively correlated with the $^{137}Cs_{\_dis\_norm}$ concentration. This was also unexpected because fine soil particles generally strongly sorb ^{137}Cs (He and Walling, 1996), so the $^{137}Cs_{\_dis\_norm}$ concentrations in river water containing large amounts of clay SS should have been lower than those in river water containing large amounts of sandy SS, as found by Smith et al. (2004). This correlation would have been caused by the clay soils mainly being on the plains, where buildings were concentrated, and because volcanic ash soils containing very extractable ^{137}Cs are mainly found on the southern plain (Takeda et al., 2013).

3.2.4. Topographic factors

The TWI was significantly and strongly and correlated with the $^{137}Cs_{\_dis\_norm}$ concentration ($r = 0.74$, Fig. 3b). Considering the hydrological discharge process, this seems to suggest that dissolved ^{137}Cs was supplied by flooding, because some studies have shown that ^{137}Cs is weakly bound to wetland soil (Valcke and Cremers, 1994) and could be the source of dissolved ^{137}Cs in the flooding area. However, the boggy area or inland water area barely covers this study area. Rather than this mechanism, this correlation is probably because buildings are mainly on the plain area and forest is mainly on steeply sloping land, because TWI is also an index of the flatness of the watershed.

Smith et al. (2004) also found that for European watersheds, the correlation between the $^{137}Cs_{\_dis\_norm}$ concentration and TWI became stronger as the proportion of the area with a high TWI value increased. The trends in Japan and Europe were similar because wetlands are mainly on plains in Europe. The main land uses on plains are different in Japan and Europe, but plains in both Japan and Europe are important sources of dissolved ^{137}Cs. Accordingly, the tendency for the $^{137}Cs_{\_dis\_norm}$ concentration in river water to be relatively high in flat areas is probably a general phenomenon, and the TWI could be a global predictor of the $^{137}Cs_{\_dis\_norm}$ concentration. This could be applied to rivers of various sizes because the watershed area is poorly correlated with the $^{137}Cs_{\_dis\_norm}$ concentration.

3.3. Multiple regression equations

The estimated parameters of the all parameter model, GIS model, and water quality model are given in Table 4. For most of the plots, the difference between the observed and predicted values was within ± 1 order of magnitude (Fig. 4). For each variable, the positive and negative values of each coefficient were consistent with those in the single correlation with $^{137}Cs_{\_dis\_norm}$ (Table 2).

In the best GIS model, the AIC value was 181.1 and the building area ratio was the primary predictor, and the clay soil ratio was selected as the second predictor. For the best water quality model, the AIC value of 192.0 was larger than that of GIS model. In this model, the EC was selected first ($p < 0.01$), and then the water temperature, DOC concentration, and pH value were selected. The best all parameter model had the smallest AIC value among the three models (AIC = 177.7). The building area ratio was selected as the primary predictor ($p = 1.4 \times 10^{-5}$). The following parameters were the soil carbon content and pH. Accordingly, the building area ratio had the greatest influence on $^{137}Cs_{\_dis\_norm}$ among the investigated candidate factors.

By comparing the AIC value of the GIS model with that of the water quality model, the GIS model had higher explanatory power than the

Table 4
Summary of the multiple regression model: effect of each variable on the normalized dissolved ^{137}Cs concentration. Identified multiple regression model for (a) all variables (all parameter model), (b) variables limited to the GIS data (GIS model), and (c) variables limited to the water quality data (water quality model). The estimated parameters for the best model are listed in order of absolute size of the effect. AIC is the Akaike information criterion, R^2 is the determination coefficient, and CI is the 95% confidence interval of each variable.

(a) All parameter model : AIC = 177.7, $R^2 = 0.67$

Predictor	Coefficient (CI)	p-value
Intercept	−2.99 (−3.20, −2.78)	
Building area ratio	1.16 (0.68, 1.64)	1.4×10^{-5}
Carbon content in soil	−0.66 (−1.15, −0.16)	9.8×10^{-4}
pH	−0.48 (−0.91, −0.04)	0.036
SS concentration	0.34 (−0.09, 0.78)	0.13

(b) GIS model : AIC = 181.1, $R^2 = 0.61$

Predictor	Coefficient (CI)	p-value
Intercept	−2.99 (−3.21, −2.77)	
Building area ratio	1.02 (0.43, 1.62)	1.4×10^{-3}
Clay soil ratio	0.71 (0.11, 1.31)	0.022

(c) Water quality model : AIC = 192.0, $R^2 = 0.54$

Predictor	Coefficient (CI)	p-value
Intercept	−2.99 (−3.23, −2.75)	
EC	0.75 (0.20, 1.30)	9.6×10^{-3}
Water temperature	0.61 (0.07, 1.15)	0.031
DOC concentration	0.54 (0.02, 1.05)	0.046
pH	−0.53 (−1.01, −0.05)	0.035

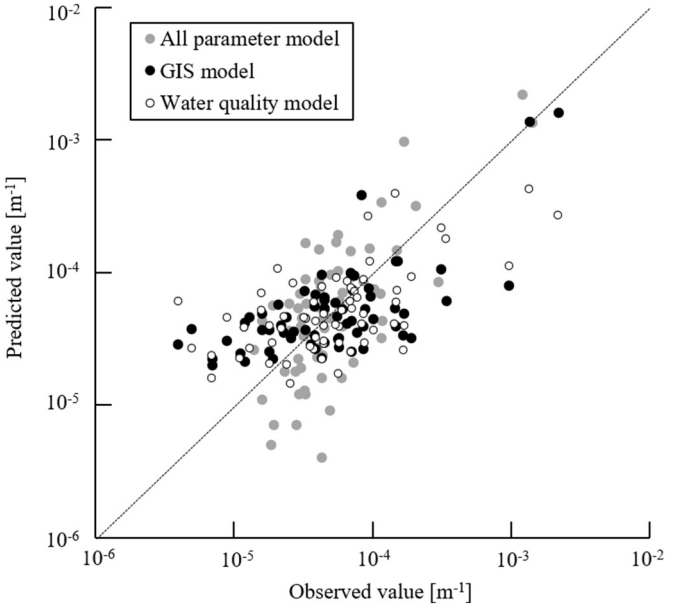

Fig. 4. Correlation between the predicted and observed normalized dissolved ^{137}Cs concentration values on the log–log scale.

water quality model, and building area ratio was the most explanatory factor overall. In addition, the water quality models could not reproduce the plots with high $^{137}Cs_{\_dis\_norm}$ values (Fig. 4). This suggests that the high $^{137}Cs_{\_dis\_norm}$ concentration in urban areas cannot be solely explained by the solid–liquid distribution of ^{137}Cs owing to the influence of the water quality, but some specific sources of ^{137}Cs would result in a relatively high $^{137}Cs_{\_dis\_norm}$ concentration. Dissolution of ^{137}Cs from road dust or volcanic ash soil are significant factors, but identifying the main contributor is the subject of future investigation.

4. Conclusions

The dissolved ^{137}Cs concentrations in water from 66 rivers in east Japan in summer 2017 are significantly and positively correlated with the average ^{137}Cs inventories for the watersheds, and the slope of the line describing the relationship is 5.8×10^{-5} m^{-1}. By comparing with the slope values in some references, this value indicates that the dissolved ^{137}Cs concentrations in rivers around the FDNPP decreased by one order of magnitude between 2012 and 2017.

By investigating the factors that are correlated with the dissolved ^{137}Cs concentrations in the rivers, the forest area ratio shows a significant negative correlation ($r = -0.63$) and the building area ratio shows a significant positive correlation with the normalized dissolved ^{137}Cs concentration ($r = 0.82$). The TWI is also significantly and positively correlated with the normalized dissolved ^{137}Cs concentration ($r = 0.74$), and a similar result has been found for European rivers. The TWI could therefore be a global predictor of the dissolved ^{137}Cs concentration. However, the underlying mechanisms for the similar relationships are different. In Europe, inland water and bogs on plains release ^{137}Cs because ^{137}Cs weakly sorbs to organic soil, but in Japan, urban area on plains have some soluble ^{137}Cs sources or maintain the dissolved ^{137}Cs concentration by causing high concentrations of K^+ and DOC to be discharged into rivers, which can inhibit ^{137}Cs sorption to soil particles.

By constructing a multiple regression model, the building area ratio is the most important explanatory variable among the land use, soil component, and water quality data. The best regression model using the land use and soil component data has a higher determination coefficient than that using the water quality data. This indicates that the high normalized dissolved ^{137}Cs concentration value in the urban area cannot be solely explained by the solid–liquid distribution of ^{137}Cs owing to the influence of the water quality, but some specific ^{137}Cs sources in the urban area would control the dissolved ^{137}Cs concentration.

Supplementary data to this article can be found online at https://doi.org/10.1016/j.scitotenv.2019.134093.

Acknowledgments

We appreciate the advice and support provided by Dr. Keiko Tagami, Dr. Tatsuhiro Nishikiori, Dr. Tomohiro Fujita, and Dr. Mirai Watanabe. This research was conducted with the aid of Grants-in-Aid for scientific research (KAKENHI Nos. 16H01791 and 17K18341). We thank Gareth Thomas and Tim Cooper, PhD, from Edanz Group (www.edanzediting.com/ac) for editing a draft of this manuscript.

References

Carter, J., Owens, P.N., Walling, D.E., Leeks, G.J.L., 2003. Fingerprinting suspended sediment sources in a large urban river system. Sci. Tot. Environ. 314–316, 513–534. https://doi.org/10.1016/S0048-9697(03)00071-8.

Delmas, M., Garcia-Sanchez, L., Onda, Y., 2019. Factors controlling the variability of ^{137}Cs concentrations in 5 coastal rivers around Fukushima Dai-ichi power plant. J. Environ. Radioact. 204, 1–11. https://doi.org/10.1016/j.jenvrad.2019.03.013.

Eguchi, S., 2017. Behavior of radioactive cesium in agricultural environment. J. Jpn. Soc. Soil Phys. 135, 9–23 (in Japanese with English Abstract).

Evrard, O., Laceby, J.P., Lepage, H., Onda, Y., Cerdan, O., Ayrault, S., 2015. Radiocesium transfer from hillslopes to the Pacific Ocean after the Fukushima nuclear power plant accident: a review. J. Environ. Radioact. 148, 92–110. https://doi.org/10.1016/j.jenvrad.2015.06.018.

Eyrolle-Boyer, F., Boyer, P., Garcia-Sanchez, L., Metivier, J.M., Onda, Y., De Vismes, A., Cagnat, X., Boulet, B., Cossonnet, C., 2016. Behaviour of radiocaesium in coastal rivers of the Fukushima Prefecture (Japan) during conditions of low flow and low turbidity - insight on the possible role of small particles and detrital organic compounds. J. Environ. Radioact. 151 (1), 328–340. https://doi.org/10.1016/j.jenvrad.2015.10.028.

Fukuda, M., Aono, T., Yamazaki, S., Nishikawa, J., Otosaka, S., Ishimaru, T., Kanda, J., 2017. Dissolved radiocaesium in seawater off the coast of Fukushima during 2013–2015. J. Radioanal. Nucl. Chem. 311 (2), 1479–1484. https://doi.org/10.1007/s10967-016-5009-9.

Garcia-Sanchez, L., Konoplev, A.V., 2009. Watershed wash-off of atmospherically deposited radionuclides: a review of normalized entrainment coefficients. J. Environ. Radioact. 100, 774–778. https://doi.org/10.1016/j.jenvrad.2008.08.005.

He, Q., Walling, D.E., 1996. Interpreting particle size effects in the adsorption of ^{137}Cs and unsupported ^{210}Pb by mineral soils and sediments. J. Environ. Radioact. 30, 117–137. https://doi.org/10.1016/0265-931X(96)89275-7.

Hilton, J., Livens, F.R., Spezzano, P., Leonard, D.R.P., 1993. Retention of radioactive caesium by different soils in the catchment of a small lake. Sci. Tot. Environ. 129 (3), 253–266. https://doi.org/10.1016/0048-9697(93)90322-W.

Iwagami, S., Tsujimura, M., Onda, Y., Nishino, M., konuma, R., Abe, Y., Hada, M., Pun, I., Sakaguchi, A., Kondo, H., Yamamoto, M., Miyata, Y., Igarashi, Y., 2017. Temporal changes in dissolved Cs concentrations in groundwater and stream water in Fukushima after the Fukushima Dai-ichi Nuclear Power Plant accident. J. Environ. Radioact. 166, 458–465. https://doi.org/10.1016/j.jenvrad.2015.03.025.

Kakehi, S., Kaeriyama, H., Ambe, D., Ono, T., Ito, S., Shimizu, Y., Watanabe, T., 2016. Radioactive cesium dynamics derived from hydrographic observations in the Abukuma River Estuary, Japan. J. Environ. Radioact. 153, 1–9. https://doi.org/10.1016/j.jenvrad.2015.11.015.

Kato, H., Onda, Y., Xiang, G., Sanada, Y., Saito, K., 2019. Reconstruction of a Fukushima accident-derived radiocesium fallout map for environmental transfer studies. J. Environ. Radioact. https://doi.org/10.1016/j.jenvrad.2019.105996 in press.

Konoplev, A.V., Golosov, V., Laptev, G., Nanba, K., Onda, Y., Takase, T., Wakiyama, Y., Yoshimura, K., 2016. Behavior of accidentally released radiocesium in soil–water environment: looking at Fukushima from a Chernobyl perspective. J. Environ. Radioact. 151 (3), 568–578. https://doi.org/10.1016/j.jenvrad.2015.06.019.

Konoplev, A.V., Wakiyama, Y., Wada, T., Golosov, V.N., Nanba, K., Takase, T., 2018. Radiocesium in ponds in the near zone of Fukushima Dai-ichi NPP. Wat. Resources. 45 (4), 589–597. https://doi.org/10.1134/S0097807818040139.

Mikami, S., Tanaka, H., Matsuda, H., Sato, S., Hoshide, Y., Okuda, N., Suzuki, T., Sakamoto, R., Andoh, M., Saito, K., 2019. The deposition densities of radiocesium and the air dose rates in undisturbed fields around the Fukushima Dai-ichi nuclear power plant; their temporal changes for five years after the accident. J. Environ. Radioact. https://doi.org/10.1016/j.jenvrad.2019.03.017 in press.

Moore, I.D., Graysn, R.B., Ladson, A.R., 1991. Digital terrain modelling: a review of hydrological, geomorphological, and biological applications. Hydrol. Process. 5, 3–30. https://doi.org/10.1002/hyp.3360050103.

Murakami, M., Saha, M., Iwasaki, Y., Yamashita, R., Koibuchi, Y., Tsukada, H., Takada, H., Sueki, K., Yasutaka, T., 2017. Source analysis of radiocesium in river waters using road dust tracers. Chemosphere 187, 217–220. https://doi.org/10.1016/j.chemosphere.2017.08.095.

Nagao, S., Kanamori, M., Ochiai, S., Tomihara, S., Fukushi, K., Yamamoto, M., 2013. Export of ^{134}Cs and ^{137}Cs in the Fukushima river systems at heavy rains by typhoon Roke in

September 2011. Biogeosciences 10 (2), 2767–2790. https://doi.org/10.5194/bg-10-6215-2013.
Nakanishi, T., Sakuma, K., 2019. Trend of ^{137}Cs concentration in river water in the medium term and future following the Fukushima nuclear accident. Chemosphere 215, 272–279. https://doi.org/10.1016/j.chemosphere.2018.10.017.
Naulier, M., Eyrolle-Boyer, F., Boyer, P., Metivier, J.M., Onda, Y., Thiry, Y., 2017. Particulate organic matter in rivers of Fukushima: an unexpected carrier phase for radiocesiums. Sci. Tot. Environ. 579, 1560–1571. https://doi.org/10.1016/j.scitotenv.2016.11.165.
Ochiai, S., Ueda, S., Hasegawa, H., Kakiuchi, H., Akata, N., Ohtsuka, Y., Hisamatsu, S., 2015. Effects of radiocesium inventory on ^{137}Cs concentrations in river waters of Fukushima, Japan, under base-flow conditions. J. Environ. Radioact. 144, 86–95. https://doi.org/10.1016/j.jenvrad.2015.03.005.
Onodera, M., Kirishima, A., Nagao, S., Takamiya, K., Ohtsuki, T., Akiyama, D., Sato, N., 2017. Desorption of radioactive cesium by seawater from the suspended particles in river water. Chemosphere 185, 806–815. https://doi.org/10.1016/j.chemosphere.2017.07.078.
Osawa, K., Nonaka, Y., Nishimura, T., Tanoi, K., Matsui, H., Mizoguchi, M., Tatsuno, T., 2018. Quantification of dissolved and particulate radiocesium fluxes in two rivers draining the main radioactive pollution plume in Fukushima, Japan (2013–2016). Anthropocene 22, 40–50. https://doi.org/10.1016/j.ancene.2018.04.003.
R Core Team, 2018. R: A language and environment for statistical computing. R Foundation for Statistical Computing, Vienna, Austria URL. https://www.R-project.org/.
Ramzaev, V., Nikitin, A., Sevastyanov, A., Artemiev Bruk, G., Ivanov, S., 2014. Shipboard determination of radiocesium in seawater after the Fukushima accident: results from the 2011–2012 Russian expeditions to the sea of Japan and western North Pacific Ocean. J. Environ. Radioact. 135, 13–24. https://doi.org/10.1016/j.jenvrad.2014.03.016.
Shin, M., Kubota, T., Manpuku, U., Suzuki, U., Yasutaka, T., Matsunami, H., Ota, T., 2019. Behavior of radiocesium in decontaminated paddy fields in Fukushima Prefecture, Japan. Paddy Water Environ. https://doi.org/10.1007/s10333-019-00694-6 in press.
Smith, J.T., Howard, D.C., Wright, S.M., Naylor, C., Brookes, A.M., Hilton, J., Howard, B.J., 1998. Use of a satellite-derived land cover map to estimate transport of radiocaesium to surface waters. Sci. Tot. Environ. 209, 1–15. https://doi.org/10.1016/S0048-9697(97)00206-4.
Smith, J.T., Wright, S.M., Cross, M.A., Monte, L., Kudelsky, A.V., Saxén, R., Vakulovsky, S.M., Timms, D.N., 2004. Global analysis of the riverine transport of ^{90}Sr and ^{137}Cs. Environ. Sci. Technol. 38, 850–857. https://doi.org/10.1021/es0300463.
Staunton, S., Roubaud, M., 1997. Adsorption of Cs-137 on montmorillonite and illite: effect of charge compensating cation, ionic strength, concentration of Cs, K and fulvic acid. Clay Clay Miner. 45 (2), 251–260. https://doi.org/10.1346/CCMN.1997.0450213.
Staunton, S., Dumat, C., Zsolnay, A., 2002. Possible role of organic matter in radiocaesium adsorption in soils. J. Environ. Radioact. 58, 163–173. https://doi.org/10.1016/S0265-931X(01)00064-9.
Takeda, A., Tsukada, H., Nakao, A., Takaku, Y., Hisamatsu, S., 2013. Time-dependent changes of phytoavailability of Cs added to allophanic andosols in laboratory cultivations and extraction tests. J. Environ. Radiact. 122, 29–36. https://doi.org/10.1016/j.jenvrad.2013.02.005.
Tertre, E., Berger, G., Castet, S., Loubet, M., Giffaut, E., 2005. Experimental sorption of Ni^{2+}, Cs^{+}, Ln^{3+} onto a montmorillonite up to 150°C. Geochim. Cosmochim. Acta 69 (21), 4937–4948. https://doi.org/10.1016/j.gca.2005.04.024.
Tsuji, H., Kondo, Y., Kawashima, S., Yasutaka, T., 2015a. Non-destructive detection of particulate radiocesium using a non-woven fabric cartridge filter for rapid preprocessing. J. Radioanal. Nucl. Chem. 303 (3), 1803–1810. https://doi.org/10.1007/s10967-014-3800-z.
Tsuji, H., Yasutaka, T., Kawabe, Y., Onishi, T., Komai, T., 2015b. Distribution of dissolved and particulate radiocesium concentrations along rivers and the relations between radiocesium concentration and deposition after the nuclear power plant accident in Fukushima. Water Res. 60, 15–27. https://doi.org/10.1016/j.watres.2014.04.024.
Tsuji, H., Nishikiori, T., Yasutaka, T., Watanabe, M., Ito, S., Hayashi, S., 2016. Behavior of dissolved radiocesium in river water in a forested watershed in Fukushima Prefecture. J. Geophys. Res. Biogeosci. 121 (10), 2588–2599. https://doi.org/10.1002/2016JG003428.
Tsuji, H., Tanaka, A., Komatsu, K., Kohzu, A., Matsuzaki, S.S., Hayashi, S., 2019. Vertical/spatial movement and accumulation of ^{137}Cs in a shallow lake in the initial phase after the Fukushima Daiichi nuclear power plant accident. Appl. Radiat. Isot. 147, 59–69. https://doi.org/10.1016/j.apradiso.2019.02.009.
Tsukada, H., Nihira, S., Watanabe, T., Takeda, S., 2017. The ^{137}Cs activity concentration of suspended and dissolved fractions in irrigation waters collected from the 80 km zone around TEPCO's Fukushima Daiichi Nuclear Power Station. J. Environ. Radioact. 178–179, 354–359. https://doi.org/10.1016/j.jenvrad.2017.08.002.
Ueda, S., Hasegawa, H., Kakiuchi, H., Akata, N., Ohtsuka, Y., Hisamatsu, S., 2013. Fluvial discharges of radiocaesium from watersheds contaminated by the Fukushima Dai-ichi Nuclear Power Plant accident, Japan. J. Environ. Radioact. 118, 96–104. https://doi.org/10.1016/j.jenvrad.2012.11.009.
Valcke, E., Cremers, A., 1994. Sorption-desorption dynamics of radiocaesium in organic matter soils. Sci. Total Environ. 157, 275–283.
Wakiyama, Y., Konoplev, A., Wada, T., Takase, T., Byrnes, I., Carradine, M., Nanba, K., 2017. Behavior of ^{137}Cs in ponds in the vicinity of the Fukushima Dai-ichi nuclear power plant. J. Environ. Radioact. 178–179, 367–376. https://doi.org/10.1016/j.jenvrad.2017.07.017.
Wauters, J., Elsen, A., Cremers, A., Konoplev, A.V., Bulgakov, A.A., Comans, R.N.J., 1996. Prediction of solid/liquid distribution coefficients of radiocaesium in soils and sediments. Part one: a simplified procedure for the solid phase characterization. Appl. Geochem. 11 (4), 589–594. https://doi.org/10.1016/0883-2927(96)00027-3.
Wu, J., Li, B., Liao, J., Feng, Y., Zhang, D., Zhao, J., Wen, W., Yang, Y., Liu, N., 2009. Behavior and analysis of cesium adsorption on montmorillonite mineral. J. Environ. Radioact. 100, 914–920. https://doi.org/10.1016/j.jenvrad.2009.06.024.
Yamashita, R., Murakami, M., Iwasaki, Y., Shibayama, N., Sueki, K., Saha, M., Mouri, G., Lamxay, S., Haechong, O., Koicuchi, Y., Takada, H., 2015. Temporal variation and source analysis of Radiocesium in an Urban River after the 2011 nuclear accident in Fukushima, Japan. J. Water and Environ. Technol. 13, 179–194. https://doi.org/10.2965/jwet.2015.179.
Yasutaka, T., Miyazu, S., Kondo, Y., Tsuji, H., Arita, K., Hayashi, S., Takahashi, A., Kawamoto, T., Aoyama, M., 2016. Development of a copper-substituted, Prussian blue-impregnated, nonwoven cartridge filter to rapidly measure radiocesium concentration in seawater. J. Nucl. Sci. 53 (9), 1243–1250. https://doi.org/10.1080/00223131.2015.1135302.
Yoshikawa, N., Obara, H., Ogasa, M., Miyazu, S., Harada, N., Nonaka, M., 2014. ^{137}Cs in irrigation water and its effect on paddy fields in Japan after the Fukushima nuclear accident. Sci. Tot. Environ. 481, 252–259. https://doi.org/10.1016/j.scitotenv.2014.01.129.
Yoshimura, K., Onda, Y., Sakaguchi, A., Yamamoto, M., Matsuura, Y., 2015. An extensive study of the concentrations of particulate/dissolved radiocaesium derived from the Fukushima Dai-ichi Nuclear Power Plant accident in various river systems and their relationship with catchment inventory. J. Environ. Radioact. 139, 370–378. https://doi.org/10.1016/j.jenvrad.2014.08.021.

Referred website

Ministry of Land, Infrastructure and Transport and Tourism, Japan, ,. National Land Numerical Information Download service. http://nlftp.mlit.go.jp/ksj/index.html, Accessed date: 23 August 2018.
Ministry of Education, Culture, Sports, Science and Technology, Japan, 2011l. Results of Airborne Monitoring Survey by MEXT in Iwate, Shizuoka, Nagano, Yamanashi, Gifu, and Toyama Prefectures, and Revision of the past airborne monitoring Results by reflecting the influences of natural radionuclides.
https://radioactivity.nsr.go.jp/en/contents/4000/3177/24/1270_111114.pdf, Accessed date: 12 May 2019.
National Institute of Advanced Science and Technology, d. Geological Survey of Japan, METI AIST satellite Data Archive System. https://gbank.gsj.jp/madas/?lang=en, Accessed date: 9 January 2019.
World Soil Information, d. Soil Grids. https://soilgrids.org, Accessed date: 10 January 2019.